Proton-Proton Elastic Scattering at LHC and Proton Structure

M. M. Islam[1], *Jan Kašpar*[2,3], *R. J. Luddy*[1], *A. V. Prokudin*[4]

[1]Department of Physics, University of Connecticut, Storrs, CT 06269 USA
[2]CERN, 1211 Genève 23, Switzerland
[3]Academy of Sciences of the Czech Republic, Prague, Czech Republic
[4]Department of Theoretical Physics, University of Torino and INFN, Torino, Italy

Talk presented by R. J. Luddy

A systematic phenomenological investigation of high energy pp and $\bar{\text{p}}$p elastic scattering has led to a physical picture of the proton. The proton appears to consist of an outer region of q$\bar{\text{q}}$ condensed ground state, an inner shell of topological baryonic charge and a core where valence quarks are confined. It is, therefore, a 'chiral bag' (a low energy model of nucleon structure) enclosed by the q$\bar{\text{q}}$ condensed state – a 'Condensate Enclosed Chiral Bag'. Based on this picture, we predict pp elastic $d\sigma/dt$ at LHC at $\sqrt{s}$= 14 TeV and $|t|$=0 – 10 GeV^2 and compare our prediction with those of a number of leading models. Precise measurement of $d\sigma/dt$ by the TOTEM Collaboration will be able to distinguish between these models.

High energy proton-proton (pp) and antiproton-proton ($\bar{\text{p}}$p) elastic scattering measurements have been at the frontier of accelerator research since the early seventies, when pp elastic scattering was measured at the CERN ISR Collider over a wide range of energy and momentum transfer. This was followed by measurement of pp elastic scattering at the Fermilab in a fixed target experiment, then by $\bar{\text{p}}$p elastic scattering measurements at the CERN Super Proton Synchrotron (SPS) Collider and, finally, in the nineties by $\bar{\text{p}}$p elastic scattering measurement at the Fermilab Tevatron. Table 1 chronicles this sustained and dedicated experimental effort by physicists extending over quarter of a century as the centre-of-mass (c.m.) energy increased from the GeV region to the TeV region. With the start-up of the LHC on the horizon, a detailed plan has been underway to measure pp elastic scattering at c.m. energy 14 TeV (seven times the c.m. energy of the Tevatron) over a wide range of momentum transfer ($|t| \simeq 0.003$ – 10.0 GeV^2) by the TOTEM Collaboration. On the other hand, the ATLAS Collaboration plans to measure pp elastic scattering at 14 TeV in the very small momentum transfer range ($|t| \simeq 0.0006$ – 0.1 GeV^2), where the pp Coulomb amplitude and strong interaction amplitude interfere.

A phenomenological investigation of high energy pp and $\bar{\text{p}}$p elastic scattering was begun by Islam et al. in the late seventies with the goal to quantitatively describe the measured elastic differential cross sections – as the c.m. energy increased and as one proton probed the other at smaller and smaller distances (when the momentum transfer increased). This investigation has now been pursued for three decades and has led to: 1) a physical picture of the proton, and 2) an effective field theory model underlying that picture [1]. The proton appears to have three regions (Fig. 1): an outer region of quark-antiquark (q$\bar{\text{q}}$) condensed ground state, an inner shell

Accelerator	$\sqrt{s}$	$\|t\|$	Reference
CERN ISR (pp)	23 - 62 GeV	0.8 - 10 GeV^2	Nagy et al. Nucl. Phys. B 150, 221 (1979)
Fermilab Fixed target (pp)	27.4 GeV	5.5 - 14.2 GeV^2	Faissler et al. Phys. Rev. D 23, 33 (1981)
CERN SPS ($\bar{p}$p)	546 GeV	0.03 - 1.55 GeV^2	Bozzo et al. Phys. Lett. B 147, 385 (1984); ibid. 155, 197 (1985)
	630 GeV	0.7 - 2.2 GeV^2	Bernard et al. Phys. Lett. B 171, 142 (1986)
	541 GeV	0.00075 - 0.120 GeV^2	Augier et al. Phys. Lett. B 316, 448 (1993)
Tevatron ($\bar{p}$p)	1.8 TeV	0.03 - 0.63 GeV^2	Amos et al. Phys. Lett. B 247, 127 (1990) Abe et al. Phys. Rev. D 50, 5518 (1994)
LHC (pp)	14 TeV	0.003 - 10 GeV^2	TOTEM Collab. Anelli et al. JINST 3 S08007 (2008)
LHC (pp)	14 TeV	0.0006 - 0.1 GeV^2	ATLAS ALFA: ATLAS Collab. TDR CERN/LHCC/2007

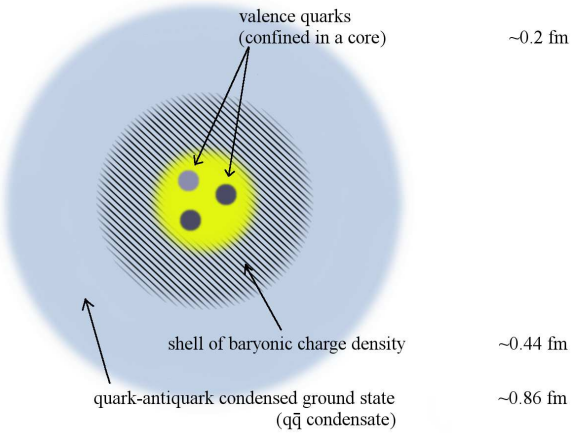

Figure 1: Physical picture of the proton – a condensate enclosed chiral bag.

of baryonic charge - where the baryonic charge is geometrical or topological in nature (similar to the 'Skyrmion Model' of the nucleon) and a core region of size 0.2 fm - where valence quarks are confined. The part of the proton structure comprised of a topological baryonic charge shell and three valence quarks in a small core has been known as a chiral bag model of the nucleon in low energy studies [2]. What we are finding from high energy elastic scattering then– is that the proton is a 'Condensate Enclosed Chiral Bag'.

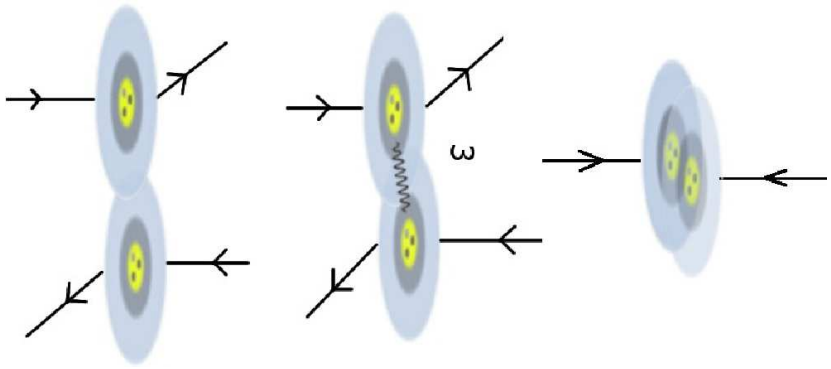

Figure 2: Elastic scattering processes (from left to right): 1) diffraction, 2) ω exchange, 3) short-distance collision ($b \lesssim 0.1$ fm).

The proton structure shown in Fig. 1 leads to three main processes in elastic scattering (Fig. 2): 1) In the small $|t|$ region, i.e., in the near forward direction, the outer cloud of $q\bar{q}$ condensate of one proton interacts with that of the other giving rise to diffraction scattering. This process underlies the observed increase of the total cross section with energy and the equality of pp and $\bar{p}p$ total cross sections at high energy. It also leads to diffraction minima, as in optics, which can be seen in our Fig. 7. 2) In the intermediate momentum transfer region ($|t| \simeq 1$ – 4 GeV^2), the topological baryonic charge of one proton probes that of the other via vector meson ω exchange. This process is analogous to one electric charge probing another via photon exchange. The spin-1 ω acts like a photon – because of its coupling with the topological baryonic charge. 3) In the large $|t|$ region: $|t| \gtrsim 4$ GeV^2, one proton probes the other at transverse distances $b \lesssim 1/q$ ($q = \sqrt{|t|}$), i.e., at transverse distances of the order of 0.1 fm or less. Elastic scattering in this region is viewed in our model as the hard collision of a valence quark from one proton with a valence quark from the other proton as shown in Fig. 3. We refer to elastic scattering with $|t| \gtrsim 4$ GeV^2 as deep-elastic scattering.

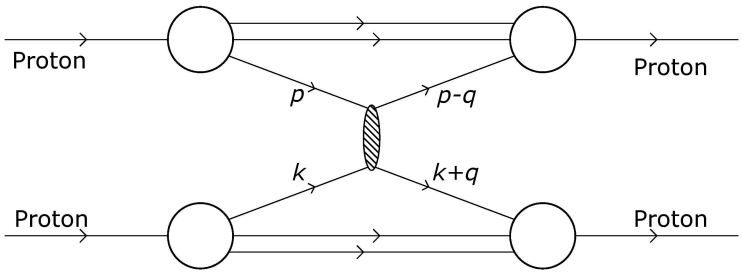

Figure 3: Hard collision of a valence quark of 4–momentum p from one proton with a valence quark of 4–momentum k from the other proton, where the collision carries off the whole momentum transfer q.

Let us next see how the above three processes are described in our calculations. Diffraction is described by using the impact parameter representation and a phenominological profile function:

$$T_D(s,t) = i\,p\,W \int_0^\infty b\,\mathrm{d}b\; J_0(b\,q)\Gamma_D(s,b); \qquad (1)$$

q is the momentum transfer ($q = \sqrt{|t|}$) and $\Gamma_D(s,b)$ is the diffraction profile function, which is related to the eikonal function $\chi_D(s,b)$: $\Gamma_D(s,b) = 1 - \exp(i\chi_D(s,b))$. We take $\Gamma_D(s,b)$ to be an even Fermi profile function:

$$\Gamma_D(s,b) = g(s)[\tfrac{1}{1+e^{(b-R)/a)}} + \tfrac{1}{1+e^{-(b+R)/a}} - 1]. \tag{2}$$

The parameters R and a are energy dependent: $R = R_0 + R_1(\ln s - \frac{i\pi}{2}\ )$, $a = a_0 + a_1(\ln s - \frac{i\pi}{2})$; $g(s)$ is a complex crossing even energy-dependent coupling strength.

The diffraction amplitude we obtain has the following asymptotic properties:

1. $\sigma_{\rm tot}(s) \sim (a_0 + a_1 \ln s)^2$ (Froissart-Martin bound)
2. $\rho(s) \simeq \frac{\pi a_1}{a_0 + a_1 \ln s}$ (derivative dispersion relation)
3. $T_D(s,t) \sim i\ s\ \ln^2 s\ f(|t|\ \ln^2 s)$ (Auberson-Kinoshita-Martin scaling)
4. $T_D^{\bar{\rm p}{\rm p}}(s,t) = T_D^{\rm pp}(s,t)$ (crossing even)

Incidentally, the profile function (2) has been used by Frankfurt et al. to estimate the absorptive effect of soft hadronic interactions (gap survival probability) in the central production of Higgs at LHC [3].

The ω-exchange amplitude in our model is given by

$$T_\omega(s,t)\ =\ \pm\tilde{\gamma}\exp[i\ \hat{\chi}(s,0)]\ s\ \tfrac{F^2(t)}{m_\omega^2 - t}, \tag{3}$$

where the $\pm$ signs refer to $\bar{\rm p}{\rm p}$ and pp scattering. The factor of s shows that ω behaves like an elementary spin-1 boson, while the two form factors indicate ω is probing two baryonic charge distributions – one for each proton. The factor $\exp[i\ \hat{\chi}(s,0)]$ comes from absorption due to the cloud-cloud interaction in ω exchange (Fig. 2).

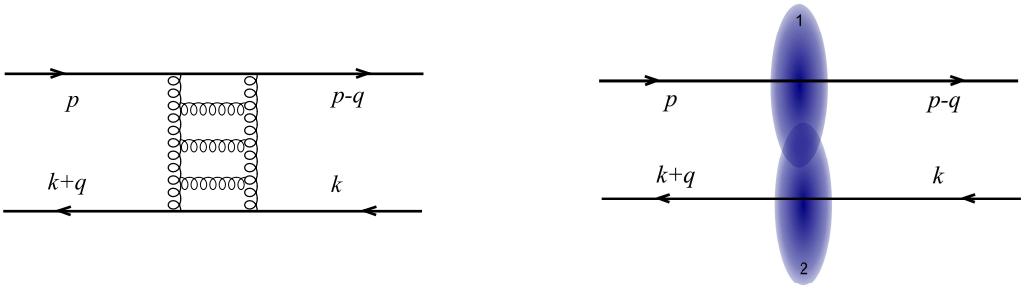

Figure 4: QCD processes for valence quark–quark scattering: (left) exchange of gluons in the form of ladders; (right) low–x gluon cloud of one quark interacting with that of the other.

For deep-elastic qq scattering, we have considered two QCD processes: Fig. 4. The first involves the exchange of reggeized gluon ladders (a BFKL ladder): figure on the left, plus next-to-leading-order corrections. We refer to this process as 'hard pomeron' exchange. Our hard pomeron amplitude is given by [4]

$$\hat{T}(\hat{s},t) = i\ \gamma_{hp}\ \hat{s}\ \left(\hat{s}\ e^{-i\frac{\pi}{2}}\right)^\omega \frac{1}{\left(1+\frac{q^2}{m_h^2}\right)}. \tag{4}$$

The energy dependence of this amplitude goes like $\hat{s}^{1+\omega}$, where $\hat{s}$ is the c.m. energy squared of the two colliding valence quarks. $\hat{s} = (p+k)^2$ and $\omega = 0.13 - 0.18$ [5]. We have used the value $\omega = 0.15$ in our calculations.

The other QCD process we have considered in Fig. 4 is where the low-x gluon cloud of one

quark interacts with that of the other: figure on the right. The corresponding amplitude is given by [6]

$$\hat{T}(\hat{s},t) = i\ \gamma_{gg}\ \hat{s}\ \left(\hat{s}\ e^{-i\frac{\pi}{2}}\right)^{\lambda} \frac{1}{\left(1+\frac{q^2}{m^2}\right)^{2(\mu+1)}}. \tag{5}$$

Its energy dependence goes like $\hat{s}^{1+\lambda}$, where λ was found to be 0.29 by Golec-Biernat and Wüsthoff (GBW Model) [7]. We used this value in our calculations.

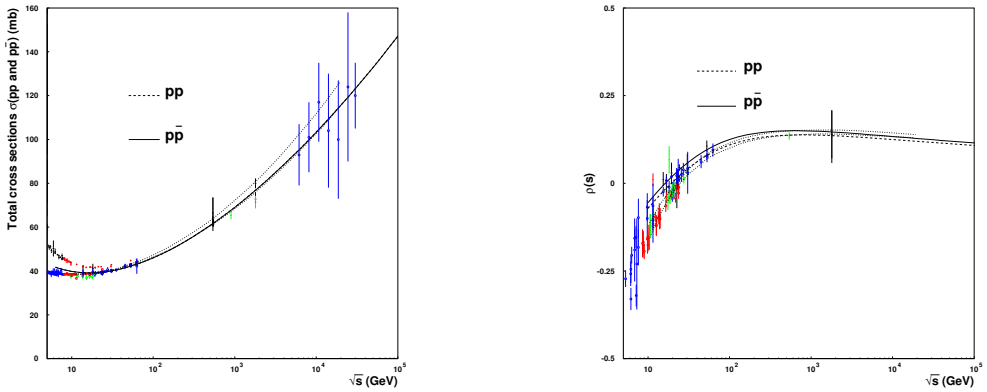

Figure 5: Left figure shows our calculated total cross section $\sigma_{tot}(s)$ as a function of $\sqrt{s}$ (solid curve). Right figure shows our calculated $\rho_{\bar{p}p}$ (solid curve) and ρ_{pp} (dashed curve) as functions of $\sqrt{s}$.

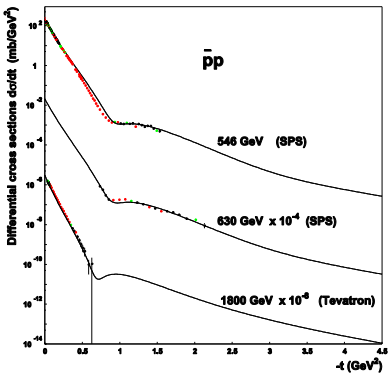

Figure 6: Solid curves show our calculated $d\sigma/dt$ at $\sqrt{s} = 546$ GeV, 630 GeV and 1.8 TeV.

The parameters in our model are determined by requiring that the model should describe satisfactorily the asymptotic behaviour of $\sigma_{tot}(s)$ and $\rho(s)$ as well as the measured $\bar{p}p$ elastic $d\sigma/dt$ at $\sqrt{s}$= 546 GeV, 630 GeV, and 1.8 TeV. The results of this investigation together with the experimental data are presented in Figs. 5 and 6 [1]. We obtain quite satisfactory descriptions. The dotted curves in Fig. 5 represent the error bands given by Cudell et al. (COMPETE Collaboration) to their best fit [8].

Our predicted pp elastic $d\sigma/dt$ at c.m. energy 14 TeV due to the combined three processes– diffraction, ω exchange, and valence quark-quark scattering (from hard pomeron exchange)

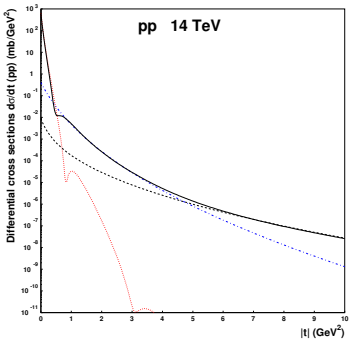

Figure 7: The solid curve shows our predicted $d\sigma/dt$ at LHC at $\sqrt{s} = 14$ TeV due to the combined three processes– diffraction, ω exchange, and valence quark–quark scattering (from hard pomeron exchange). Also shown are separate $d\sigma/dt$'s due to diffraction (dotted curve), ω exchange (dot–dashed curve), and valence quark–quark scattering (dashed curve).

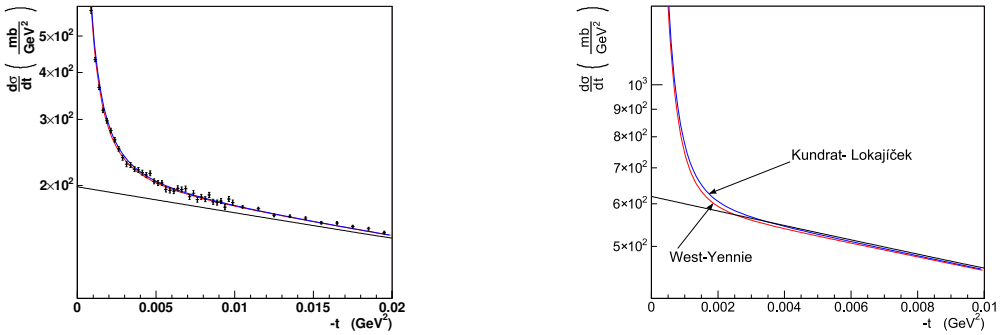

Figure 8: Left figure shows our calculated $d\sigma/dt$ for $\bar{p}p$ elastic scattering at $\sqrt{s} = 541$ GeV in the Coulomb–hadronic interference region together with the experimental data[11]. Right figure presents our predicted $d\sigma/dt$ for pp elastic scattering at $\sqrt{s} = 14$ TeV in the Coulomb–hadronic interference region.

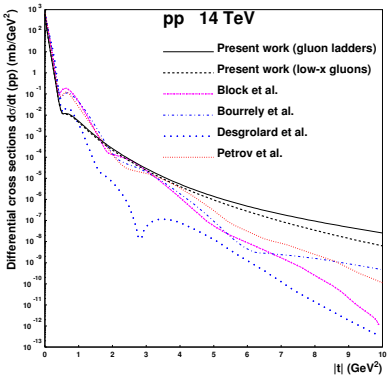

Figure 9: Our predicted $d\sigma/dt$ at LHC at c.m. energy 14 TeV with q–q scattering due to gluon ladders (solid curve) and low–x gluon cloud–cloud interaction (dashed curve). Also shown are predicted $d\sigma/dt$ of four other dynamical models [12, 13, 14, 15].

is shown in Fig. 7 [1]. Also shown are separate $d\sigma/dt$'s due to diffraction (dotted curve), ω exchange (dot-dashed curve), and valence quark-quark scattering (dashed curve). At $\sqrt{s} = 14$ TeV, our calculated values for σ_{tot} and $\rho_{\rm pp}$ are 110 mb and 0.120, respectively.

Fig. 8 (left) shows our calculated $d\sigma/dt$ for $\bar{\rm p}$p elastic scattering at $\sqrt{s} = 541$ GeV [1] in the Coulomb-hadronic interference region using the Kundrát–Lokajíček formulation [9] and the West-Yennie formulation [10]. Experimental data are from Augier et al. [11]. Right figure in Fig. 8 presents our predicted $d\sigma/dt$ for pp elastic scattering at $\sqrt{s} = 14$ TeV [1] in the Coulomb-hadronic interference region using the Kundrát–Lokajíček formulation (upper curve) and the West-Yennie formulation (lower curve). The straight lines in Fig. 8 represent $d\sigma/dt$ due to our hadronic amplitude by itself. The ATLAS ALFA experiment plans to measure pp $d\sigma/dt$ in this region at LHC.

Finally, in Fig. 9, we show our predicted pp elastic $d\sigma/dt$ at $\sqrt{s} = 14$ TeV with quark-quark scattering due to hard pomeron exchange (solid line) and due to low-x gluon cloud-cloud interaction (dashed line) and compare with the predicted $d\sigma/dt$ of four other dynamical models [12, 13, 14, 15]. A distinctive feature of our predicted $d\sigma/dt$ is that the differential cross section falls off smoothly beyond the bump at $|t| \simeq 1$ GeV^2. In contrast, the other models predict visible oscillations in $d\sigma/dt$. Furthermore, these models lead to much smaller differential cross sections than ours in the large $|t|$ region: $|t| \gtrsim 5$ GeV^2.

If the planned measurement of elastic $d\sigma/dt$ by the TOTEM Collaboration in the momentum transfer range $|t| \simeq 0 - 10$ GeV^2 shows quantitative agreement with our predicted $d\sigma/dt$, then the underlying picture of the proton–a 'Condensate Enclosed Chiral Bag' (as shown in Fig. 1) will be supported. The consequent discovery of the structure of the proton at LHC at the beginning of the 21st century will be analogous to the discovery of the structure of the atom from high energy α- particle scattering by gold atoms at the beginning of the 20th century.

Acknowledgements

The authors wish to thank the members of the TOTEM Collaboration for discussions and comments. MMI and RJL would like to thank CERN for Conference support. RJL would also like to thank Northwest Catholic High School for travel support.

References

[1] M. M. Islam, R. J. Luddy and A. V. Prokudin, *Int. J. Mod. Phys. A***21**, 1 (2006).
[2] A. Hosaka and H. Toki: *Quarks, Baryons and Chiral Symmetry*, World Scientific Publishing Co. (2001).
[3] L. Frankfurt, C. E. Hyde-Wright, M. Strikman and C. Weiss, *Phys. Rev. D* **75**, 054009 (2007).
[4] M. M. Islam, R. J. Luddy and A. V. Prokudin, *Phys. Lett. B* **605**, 115 (2005).
[5] S. Brodsky, V. S. Fadin, V. T. Kim, L. N. Lipatov and G. B. Pivovarov, *JETP Lett.* **70**, 155 (1999).
[6] M. M. Islam, Jan Kašpar and R. J. Luddy, *Mod. Phys. Lett. A* **24**, 485 (2009).
[7] K. Golec-Biernat and M. Wüsthoff, *Phys. Rev. D* **59**, 014017 (1998); *ibid.* **60**, 114023 (1999).
[8] J. R. Cudell *et al.*, COMPETE Collab.,*Phys. Rev. Lett.* **89**, 201801 (2002).
[9] V. Kundrát and M. Lokajíček, *Z. Phys. C* **63**, 619 (1994).
[10] G. B. West and D. R. Yennie, *Phys. Rev.* **172**, 1413 (1968).
[11] C. Augier *et al.*, *Phys. Lett. B* **316**, 448 (1993).
[12] M. M. Block, E. M. Gregores, F. Halzen and G. Pancheri, *Phys. Rev. D* **60**, 054024 (1999).
[13] C. Bourrely, J. Soffer and T. T. Wu, *Eur. Phys. J. C* **28**, 97 (2003).
[14] P. Desgrolard, M. Giffon, E. Martynov and E. Predazzi, *Eur. Phys. J. C* **16**, 499 (2000).
[15] V. Petrov, E. Predazzi and A. V. Prokudin, *Eur. Phys. J. C* **28**, 525 (2003).